PHYSICAL REVIEW B **84**, 140405(R) (2011)

Dispersion of collective magnonic modes in stacks of nanoscale magnetic elements

M. Dvornik and V. V. Kruglyak
School of Physics, University of Exeter, Exeter, EX4 4QL, United Kingdom
(Received 4 July 2011; revised manuscript received 15 August 2011; published 5 October 2011)

We report a numerical study of the dispersion of collective magnonic modes in magnonic crystals formed by stacks of magnetostatically coupled magnetic nanoelements. The calculations reveal that the sign of the magnonic dispersion is determined by the spatial character and ellipticity of precession for the eigenmodes of the isolated elements that give rise to the magnonic bands. We identify a critical value of the ellipticity at which the dispersion of the collective magnonic modes changes sign. The critical value is independent of the magnetic parameters and shape of the elements but is a characteristic of their arrangement (superstructure).

DOI: 10.1103/PhysRevB.84.140405 PACS number(s): 75.30.Ds, 75.78.Cd, 75.75.Jn

The recent renaissance of interest in magnonic crystals[1]—media with periodic modulation of magnetic parameters—has led to several important advances in the understanding of propagation, confinement, and quantization of spin waves[2] in magnetostatically coupled one-dimensional (1D)[3] and two-dimensional (2D)[4] arrays of magnetic elements as well as 2D arrays of antidots (holes in otherwise continuous films).[5] In contrast to the numerous studies of spin waves confined in continuous nano- and microscale magnetic elements,[6–8] magnonics[9] has emerged as a field aiming at the investigation of propagating spin waves in nanostructured magnetic samples, with a promise of reprogrammable magnetoelectronic devices.[9–11]

The outlined progress is, however, in striking contrast to studies of nano- and microscale magnetic elements in three dimensions (3D). Experimentally, the situation is due to the lack of adequate techniques.[9] On the other hand, numerical micromagnetic modeling[12,13] is limited by available computing power. The analytical theory has shown most progress,[14–16] yet with only the simplest models addressed so far.

In this Rapid Communication, we present a numerical study of collective magnonic modes in stacks of thin magnetic nanoelements. The spectrum, dispersion, and spatial character of magnonic modes are extracted from simulations performed using the object-oriented micromagnetic framework (OOMMF)[17] and thoroughly analyzed. The calculations reveal that the sign of the dispersion within magnonic bands is determined by the spatial character and ellipticity of the modes of the isolated element that give rise to the bands. In particular, we find that, in our sample, the magnonic bands originating from the edge and quasiuniform delocalized (fundamental) modes have negative dispersion, while the higher-order delocalized modes give rise to bands with positive dispersion. Moreover, we have identified a critical value of the ellipticity at which the magnonic dispersion changes its sign. We demonstrate that the critical value of the ellipticity is defined by the properties of the magnetodipolar interaction.

The simulations were performed for stacks of 60 and 240 elements formed by rectangular $L \times 50 \times 10$ nm^3 elements with rounded corners, with a radius of curvature of 10 nm and length L ranging from 30 to 200 nm (see Fig. 1). The element-to-element separation is 10 nm. The magnetic parameters are close to those of permalloy,[18] with the magnetic anisotropy neglected and the value of the Gilbert damping constant reduced to 10^{-4}. The discretization cell was set to $2.5 \times 2.5 \times 10$ nm^3, i.e., each element was one cell thick. The magnetic ground states of the samples were prepared by quasiadiabatic relaxation from the perfect saturation tilted in plane by 10° from the x axis, first at the field of 3000 Oe, and then in 10-Oe steps, to the state at the bias field H_b of 1500 Oe.

In the dynamical simulations, the samples were excited by a small broadband magnetic field, localized in the center of the stack and directed along the z axis and uniform in the (x,y) plane. Dynamical states $\mathbf{M}(\mathbf{r},t)$ were recorded every 10 ps within the first 80 ns of each simulation and used to calculate cellwise Fourier spectra with the discrete Fourier transform (DFT). The frequencies of individual modes were extracted by fitting peaks in the sum of DFT amplitude spectra from all cells of the sample to the Lorentzian function. The spatial profiles of the amplitude and phase of individual modes at fitted frequencies were then reconstructed from the cellwise DFT data.

To calculate the dispersion of spin waves in the 3D samples studied here, we have extended the method developed for the 1D case in Ref. 12. The results were visualized by applying the four-dimensional (4D) DFT to the entire simulated (in real space and time) data set, and then summing the obtained Fourier amplitudes in the reciprocal space over the (k_x,k_y) plane for each value of k_z. The 2D representation of the spin-wave dispersion obtained in this way contained contributions from both symmetric and antisymmetric modes.

The inset of Fig. 2 shows a typical spectrum of spin waves excited in the isolated $100 \times 50 \times 10$ nm^3 element, with three dominant modes observed in the frequency range of 30 GHz. The two lowest-frequency modes are the "edge" and "bulk" modes, respectively, discussed, e.g., in Ref. 13. The highest-frequency mode shown is a higher-order "bulk" mode, with further higher-order modes observed beyond the shown frequency range. For the edge mode, the ellipticity of precession is very small ($m_z/m_y \ll 1$, where m_z and m_y are components of the dynamic magnetization). For the fundamental bulk mode, dynamics is still dominated by the in-plane component ($m_z/m_y \approx 0.5$). Finally, for the higher-order bulk mode, the out-of-plane and in-plane components of the dynamic magnetization are of the same order of magnitude ($m_z/m_y \approx 1$).

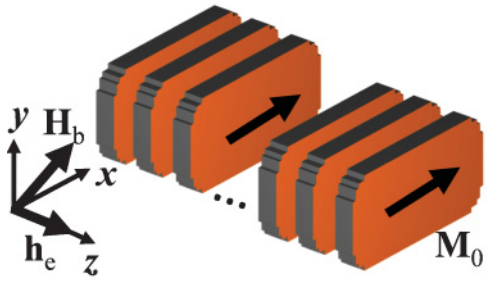

FIG. 1. (Color online) The geometry of the problem is shown schematically. The inset shows the coordinate system used in the calculations, together with the orientations of the bias and excitation magnetic fields.

The frequencies of the modes of different character are summarized in Fig. 2 as a function of their ellipticities for the different elements. Generally, the ellipticity of the modes of the isolated element increases as their frequency increases. The ellipticity of the lower-frequency modes is defined mainly by the anisotropic dipolar energy, leading to a noncircular precession. At higher frequencies, the dynamics is dominated by the isotropic exchange interaction, and so the precession is almost circular. Generally, the ellipticity of the fundamental bulk mode decreases as the size of the element increases, which could be understood by the increasing shape anisotropy and decreasing exchange interaction. In turn, the ellipticity of the edge mode increases with the size of the element, which could be attributed to changes of the mode profile.

In stacks, the magnetodipolar coupling between elements splits modes of the isolated element into bands of collective magnonic modes (Fig. 3). The frequencies of the collective modes in the center of the Brillouin zone [Fig. 3(a)] are generally lower than those of the corresponding modes of the isolated element (Fig. 2). This can be attributed to

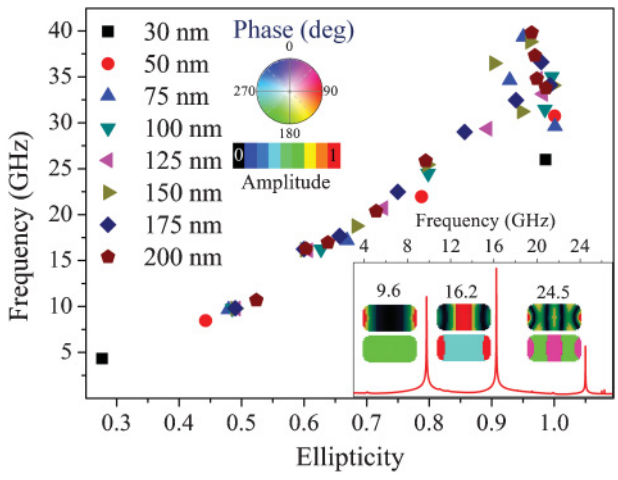

FIG. 2. (Color online) The frequencies of the modes of the isolated elements of different sizes are shown as a function of their ellipticity. In the inset, the mode spectrum of the isolated $100 \times 50 \times 10$ nm^3 element is shown. For each mode, the top and bottom images represent the spatial distributions of the DFT amplitude and phase, respectively, while the numbers are the frequencies in GHz.

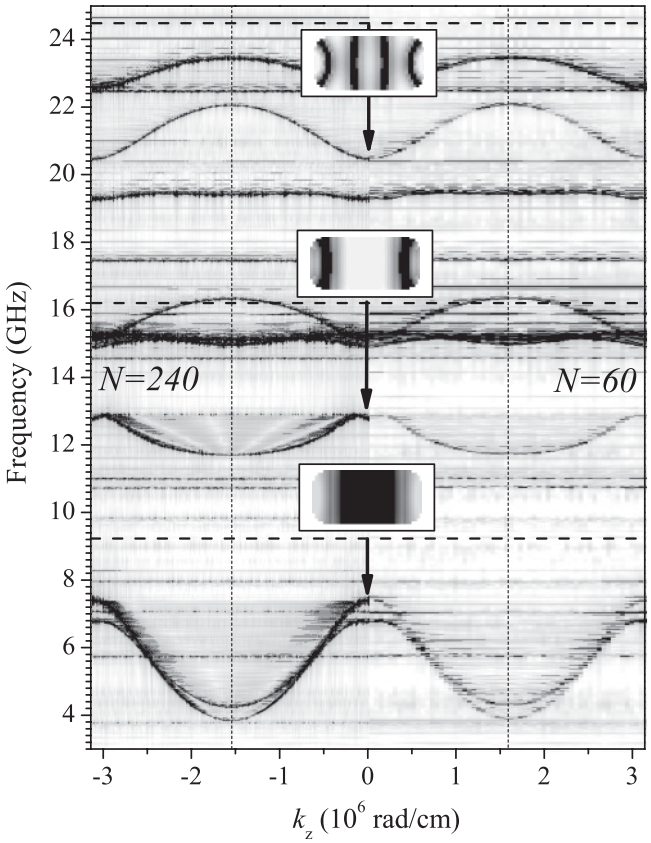

FIG. 3. The magnonic dispersion is shown for stacks of 240 (left-hand side) and 60 (right-hand side) elements with dimensions of $100 \times 50 \times 10$ nm^3. The insets show the spatial profiles of the modes of the isolated element, while the horizontal dashed lines represent their frequencies. The arrows point to the magnonic bands formed from the modes of the isolated element. The solid vertical short dashed lines show the boundaries of the Brillouin zone.

the effect of the static stray magnetodipole field from the neighbors, since the field adds up to its own demagnetizing field of each element. There are dispersive magnonic bands, which are characterized by different signs of dispersion, and also some dispersionless modes, which are represented by the horizontal lines. The intensity of the dispersionless modes is generally lower than that of the dispersive ones. This is due to the weaker coupling of the dispersionless modes to the local excitation, which can be explained by their reduced amplitude in the center of the stack.

Two dispersion branches are observed for the lowest standing mode corresponding to the edge mode of the isolated element (Fig. 2). The spatial profiles of the modes in the planes of individual elements reveal that the dispersion branches starting from the higher and lower frequencies originate from the symmetric and antisymmetric edge modes of the isolated element, respectively. The width of the band originating from the symmetric edge mode is greater than that of the antisymmetric edge modes, indicating that the stray field coupling for the antisymmetric edge modes is somewhat weaker than that for the symmetric edge modes.

For the edge and fundamental bulk modes, the collective modes at the boundaries of the Brillouin zone have frequencies

that are smaller than those of the modes in the center of the Brillouin zone, i.e., a redshift (negative dispersion) is observed. At the same time, a blueshift (positive dispersion) is observed for the higher-order bulk modes. We therefore observe either negative or positive dispersion depending on the mode profile within the individual elements.

To interpret the observation, let us consider a chain of magnetostatically coupled magnetic moments (spins). In a chain magnetized parallel (perpendicular) to its length, the static stray magnetic field from the neighbors is approximately parallel (antiparallel) to the static orientation of individual spins, thereby increasing (decreasing) the frequency of their precession for both uniform and nonuniform collective modes. In contrast, the effect of the dynamic stray field depends on the relative phase of precession of the neighboring spins and is therefore different for uniform (in the center of the Brillouin zone) and nonuniform (e.g., at the boundaries of the Brillouin zone) precession.

In the case of magnetization perpendicular to the length of the chain, which is relevant to the present study, the dynamic magnetic moment has two components—one parallel and one perpendicular to the chain. For the case of in-phase (out-of-phase) precession for the modes in the center (near the boundaries) of the Brillouin zone, the stray field due to the component of the neighbors' dynamic magnetic moment *parallel* to the chain is parallel (antiparallel) to the dynamic magnetic moment of individual elements, thereby decreasing (increasing) the frequency of their precession via decreasing (increasing) the "restoring force" acting upon the spins. In contrast, the effect of the stray field due to the component of the neighbors' dynamic magnetic moment *perpendicular* to the chain is exactly opposite.

So, the interaction due to the dynamic magnetic moments parallel and perpendicular to the chain leads to positive and negative contributions to the dispersion, respectively. The resulting dispersion of the collective modes of the chain is therefore determined by the relative strength of the two opposite effects that is, in turn, determined by the *ellipticity* of precession.

In particular, for the edge and fundamental bulk mode, the ellipticity is small, and their precession is dominated by the dynamic magnetization perpendicular to the direction of stacking, leading to the observed negative dispersion. The ellipticity is more significant for the bulk mode, leading to its weaker dispersion. In contrast, the trajectory of precession of the higher-order bulk modes is almost circular, with a significant component parallel to the direction of stacking, leading to their observed positive dispersion. The width of magnonic bands varies depending on the exact mode profile, which could, in principle, be addressed by a quantitative simultaneous account of the ellipticity, amplitude, and phase profiles of the modes as described in Ref. 13. This is, however, beyond the scope of the present study.

To quantify the effect of ellipticity on the dispersion of the collective magnonic modes, we performed additional simulations in which the size of the constitutive elements along the major axis was varied from 30 to 200 nm. The simulations were done for stacks of 60 elements, since the preliminary simulations (Fig. 3) had not revealed any significant differences in the responses of stacks of 60 and 240 elements.

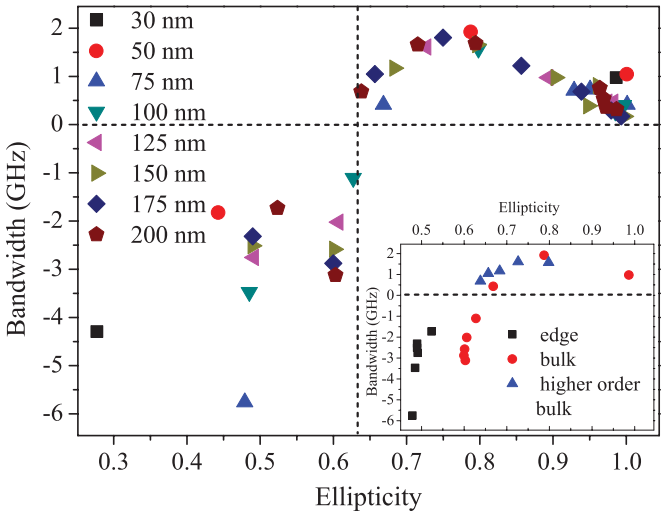

FIG. 4. (Color online) The widths of the collective magnonic bands are shown as a function of the ellipticity of the corresponding modes of the isolated elements. The inset shows the same dependence, but for the edge, bulk, and high-order bulk modes, only.

For each eigenmode of the isolated elements of each size, the weighted average value of the ellipticity was calculated as $\langle \varepsilon \rangle = \frac{\sum_V m_i (m_i^z / m_i^y)}{\sum_V m_i}$, where m_i denotes the Fourier amplitude of the given mode in the ith cell and the summation is performed over the volume of the element. Then, the widths of the corresponding magnonic bands were extracted from the dispersions calculated for the stacks of such elements, with the positive and negative values of the width values assigned to the positive and negative dispersion, respectively. The results are presented in Fig. 4.

The main feature of the data presented in Fig. 4 is the presence of the critical value of the ellipticity $\varepsilon_{\text{lim}} \approx 0.63$ above which the magnonic dispersion becomes positive. Only two modes were found to have ellipticities below the critical value. In particular, the edge mode always has ellipticity below the critical value. The fundamental bulk modes have an ellipticity below the critical value only for elements that are larger than 75 nm. Hence, by altering the dimensions of the constituent elements, it is possible to control the magnonic dispersion in the stack, at least as far as the fundamental bulk mode is concerned. The observed gradual decrease of the ellipticity of the higher-order bulk modes with the size of the element suggests that they might eventually also show negative dispersion.

The critical value of the ellipticity is found to be independent of the shape of the isolated element, suggesting that it could be related to some fundamental properties of the magnetodipole interaction. To verify this hypothesis, we applied the theory of collective modes developed in Ref. 13 to the case of a stack of two elements. In this case, each eigenmode of the isolated element will split into two normal modes of the pair—acoustical and optical modes—with frequencies of ω_+ and ω_-, respectively. The cases of $\omega_+ > \omega_-$ and $\omega_+ < \omega_-$ correspond to the regions of negative and positive dispersion, respectively. So the regions of different dispersion are separated by the point where the frequencies of the acoustical and optical modes are equal, $\omega_+ = \omega_-$.

In the dipolar approximation the latter condition leads to $\int_{V_1}\int_{V_2}\frac{[1-3(\nu_\delta^z)^2]m_z(\mathbf{r}_1)m_z(\mathbf{r}_2)+[1-3(\nu_\delta^y)^2]m_y(\mathbf{r}_1)m_y(\mathbf{r}_2)}{|\delta+\mathbf{r}_2-\mathbf{r}_1|^3}d^3\mathbf{r}_1 d^3\mathbf{r}_2 = 0$, where ν_δ^z and ν_δ^y denote the y and z components of the unit vector connecting two points of the interacting elements (for our particular case $\nu_\delta^z = 1$ and $\nu_\delta^y = 0$). Functions $m_z(\mathbf{r})$ and $m_y(\mathbf{r})$ define the spatial profile of the modes. δ is the radius vector between the centers of the interacting elements. The integration is performed over the volumes of the two elements V_1 and V_2. The equation requires that $[1-3(\nu_\delta^z)^2]m_z(\mathbf{r}_1)m_z(\mathbf{r}_2)+[1-3(\nu_\delta^y)^2]m_y(\mathbf{r}_1)m_y(\mathbf{r}_2) = 0$. If we now additionally assume that the ellipticity of the mode is spatially uniform and, in particular, $m_z(\mathbf{r}_1)/m_y(\mathbf{r}_1) = m_z(\mathbf{r}_2)/m_y(\mathbf{r}_2)$, then the critical value of the ellipticity can be easily evaluated to yield $\varepsilon = \sqrt{\frac{3(\nu_\delta^y)^2-1}{1-3(\nu_\delta^z)^2}} \approx 0.707$. The account of higher-order multipole moments would obviously change the critical value of the ellipticity. Nevertheless, the result is already very close to the one obtained from the simulations ($\approx$0.63). The calculation suggests that the critical value of the ellipticity is invariant with respect to the magnetic parameters, the shape of and the distance between the elements, but is different for different stacking geometries. In the latter case, as well as the case of 2D or 3D arrays, the critical value of the ellipticity can be derived in a similar way and used to explain the sign of the dispersion of collective magnetodipolar modes.

The mechanism of the dispersion revealed here could also be used to predict the dispersion of magnonic modes in in-plane chains of coupled magnetic elements from Ref. 19 and in those composed of elements, pairs of which we studied numerically in Ref. 13. By applying the same routine to the case of the elements placed "end to end" and magnetized along their major axis, one can find that no critical value of the ellipticity is expected and hence the dispersion is always negative. In contrast, if the elements are placed side by side, then there is a critical value of ellipticity of $\varepsilon = \sqrt{2}$, below which the dispersion is positive. One should note, however, that, due to the shape anisotropy, such a large value of the ellipticity is difficult to realize in planar elements. The additional exchange coupling between elements in magnonic waveguides such as those studied in Ref. 20 should only strengthen the positive dispersion, provided, of course, that the system would still be within the limits of the "tight-binding" approach used here.

In summary, we have studied the spectrum and dispersion of magnonic modes in stacks of dipolarly coupled magnetic elements. In particular, we have found that the sign of the magnonic dispersion is determined by the spatial character and ellipticity of the corresponding modes of an isolated element. Moreover, we have determined a critical value of the ellipticity at which the sign of the magnonic dispersion changes from negative to positive in a discontinuous way. The discovered effect suggests a way of tailoring the dispersion of collective spin waves in magnonic crystals.

The authors gratefully acknowledge fruitful discussions with B. A. Ivanov and P. Bondarenko. The research leading to these results has received funding from the EC's 7th Framework Programme (FP7/2007-2013) GA 233552 (DYNAMAG) and from the EPSRC of the UK (EP/E055087/1).

[1] S. A. Nikitov, P. Tailhades, and C. S. Tsai, J. Magn. Magn. Mater. **236**, 320 (2001).

[2] A. G. Gurevich and G. A. Melkov, *Magnetization Oscillations and Waves* (Boca Raton, FL, 1996).

[3] G. Gubbiotti, S. Tacchi, M. Madami, G. Carlotti, A. O. Adeyeye, and M. Kostylev, J. Phys. D **43**, 264003 (2010).

[4] A. Y. Galkin, B. A. Ivanov, and C. E. Zaspel, Phys. Rev. B **74**, 144419 (2006); L. Giovannini, F. Montoncello, and F. Nizzoli, *ibid.* **75**, 024416 (2007); V. V. Kruglyak, P. S. Keatley, A. Neudert, R. J. Hicken, J. R. Childress, and J. A. Katine, Phys. Rev. Lett. **104**, 027201 (2010); S. Tacchi, M. Madami, G. Gubbiotti, G. Carlotti, H. Tanigawa, T. Ono, and M. P. Kostylev, Phys. Rev. B **82**, 024401 (2010).

[5] B. Lenk, H. Ulrichs, F. Garbs, and M. Münzenberg, Phys. Rep. **507**, 107 (2011).

[6] C. Mathieu, J. Jorzick, A. Frank, S. O. Demokritov, A. N. Slavin, B. Hillebrands, B. Bartenlian, C. Chappert, D. Decanini, F. Rousseaux, and E. Cambril, Phys. Rev. Lett. **81**, 3968 (1998); G. Gubbiotti, L. Albini, G. Carlotti, M. De Crescenzi, E. Di Fabrizio, A. Gerardino, O. Donzelli, F. Nizzoli, H. Koo, and R. D. Gomez, J. Appl. Phys. **87**, 5633 (2000); Y. Roussigné, S. M. Chérif, C. Dugautier, and P. Moch, Phys. Rev. B **63**, 134429 (2001).

[7] J. Jorzick, S. O. Demokritov, B. Hillebrands, M. Bailleul, C. Fermon, K. Y. Guslienko, A. N. Slavin, D. V. Berkov, and N. L. Gorn, Phys. Rev. Lett. **88**, 47204 (2002); J. P. Park, P. Eames, D. M. Engebretson, J. Berezovsky, and P. A. Crowell, *ibid.* **89**, 277201 (2002); A. Barman, V. V. Kruglyak, R. J. Hicken, J. M. Rowe, A. Kundrotaite, J. Scott, and M. Rahman, Phys. Rev. B **69**, 174426 (2004); M. Bailleul, R. Höllinger, K. Perzlmaier, and C. Fermon, *ibid.* **76**, 224401 (2007).

[8] G. Gubbiotti, M. Conti, G. Carlotti, P. Candeloro, E. Di Fabrizio, K. Yu. Guslienko, A. Andre, C. Bayer, and A. N. Slavin, J. Phys.: Condens. Matter. **16**, 7709 (2004); M. Pardavi-Horvath, C. A. Ross, and R. D. McMichael, IEEE Trans. Magn. **41**, 3601 (2005); V. V. Kruglyak, P. S. Keatley, R. J. Hicken, J. R. Childress and J. A. Katine, Phys. Rev. B **75**, 024407 (2007).

[9] V. V. Kruglyak, S. O. Demokritov, and D. Grundler, J. Phys. D **43**, 264001 (2010), and references therein.

[10] A. Khitun, M. Q. Bao, and K. L. Wang, J. Phys. D **43**, 264005 (2010), and references therein.

[11] Y. Au, T. Davison, E. Ahmad, P. S. Keatley, R. J. Hicken, and V. V. Kruglyak, Appl. Phys. Lett. **98**, 122506 (2011).

[12] V. V. Kruglyak and R. J. Hicken, J. Magn. Magn. Mater. **306**, 191 (2006); S.-K. Kim, J. Phys. D **43**, 264004 (2010), and references therein.

[13] M. Dvornik, P. Bondarenko, B. A. Ivanov, and V. V. Kruglyak, J. Appl. Phys. **109**, 07B912 (2011).

[14] M. Krawczyk and H. Puszkarski, J. Appl. Phys. **100**, 073905 (2006).

[15]P. Chu, D. L. Mills, and R. Arias, Phys. Rev. B **73**, 094405 (2006); M. Krawczyk and H. Puszkarski, *ibid*. **77**, 054437 (2008).

[16]M. Krawczyk, J. Klos, M. L. Sokolovskyy, and S. Mamica, J. Appl. Phys. **108**, 093909 (2010).

[17]M. Donahue and D. G. Porter, OOMMF User's guide, Version 1.0, Interagency Report NISTIR 6376, NIST, 1999, [http://math.nist.gov/oommf].

[18]Magnetization of saturation $M_s = 8\times10^5$ A/m, Landé g factor $g = 2.1$, and exchange constant $A = 1.3\times10^{-11}$ J/m.

[19]J. Ding, S. Jain, and A. O. Adeyeye, J. Appl. Phys. **109**, 07D301 (2011); R. Zivieri, F. Montoncello, L. Giovannini, F. Nizzoli, S. Tacchi, M. Madami, G. Gubbiotti, G. Carlotti, and A. O. Adeyeye, Phys. Rev. B **83**, 054431 (2011).

[20]K. S. Lee, D. S. Han, and S. K. Kim, Phys. Rev. Lett. **102**, 127202 (2009); A. V. Chumak, P. Pirro, A. A. Serga, M. P. Kostylev, R. L. Stamps, H. Schultheiss, K. Vogt, S. J. Hermsdoerfer, B. Laegel, P. A. Beck, and B. Hillebrands, Appl. Phys. Lett. **95**, 262508 (2009).